

The ν -process with fully time-dependent supernova neutrino emission spectra

A. SIEVERDING,¹ K. LANGANKE,^{2,3} G. MARTÍNEZ-PINEDO,^{2,3} R. BOLLIG,⁴ H.-T. JANKA,⁴ AND A. HEGER^{5,6,7}

¹*School of Physics and Astronomy, University of Minnesota, Minneapolis, MN 55455, USA*

²*GSI Helmholtzzentrum für Schwerionenforschung, Planckstraße 1, 64291 Darmstadt, Germany*

³*Institut für Kernphysik (Theoriezentrum), Technische Universität Darmstadt, Schlossgartenstraße 2, 64289 Darmstadt, Germany*

⁴*Max-Planck-Institut für Astrophysik, Karl-Schwarzschild-Straße 1, D-85748 Garching, Germany*

⁵*Monash Centre for Astrophysics, School of Physics and Astronomy, Monash University, Victoria 3800, Australia*

⁶*Tsing-Dao Lee Institute, Shanghai 200240, China*

⁷*The Joint Institute for Nuclear Astrophysics, Michigan State University, East Lansing, Michigan 48824, USA*

ABSTRACT

The neutrino process that occurs in the outer stellar shells during a supernova explosion and involves neutrino-nucleus reactions produces a range of rare, stable and radioactive isotopes. We improve previous ν -process studies by using, for the first time, the time-dependent neutrino emission spectra, as predicted from supernova simulations, rather than a simplified parametric description modeled after the neutron-star cooling phase. In particular, our calculations use time-dependent neutrino spectra for all neutrino species, consider their deviation from a Fermi-Dirac distribution and account for the neutrino emission from the neutrino burst and accretion phases. We find that the time-dependent treatment of the neutrino emission spectra results in higher yields for the selected nuclei produced by the ν process as compared to previous studies and also compared to the approximation of assuming constant neutrino energies corresponding to the time-averaged mean energy radiated in each species. The effect is largest for nuclides produced by charged-current reactions. Our results reflect the dynamical competition between neutrino-induced reactions and the effect of the shock passage through the star. By varying the neutrino burst luminosity and the duration of the accretion phase, we study the impact of these early emission phases and their uncertainties on the ν -process nucleosynthesis. We find that the deviation of the neutrino spectra from a Fermi-Dirac distribution calculated in supernova simulations has a negligible effect on the ν -process yields.

Keywords: neutrino nucleosynthesis, core-collapse supernova

1. INTRODUCTION

Supernova explosions are not only among the brightest observable events in the universe, they are also the key mechanism to allow the products of stellar nucleosynthesis to contribute to the chemical enrichment of the galaxy. Even though the majority of the nuclei that constitute the final ejecta of such an explosion are already formed during the hydrostatic burning phases, the explosion itself leaves an imprint on the final composition. Explosive Si, O, and Ne burning are important for the production of the elements between carbon and iron. Furthermore, this hot, shock heated environment allows the production of light and heavy p nuclei by the γ process (Woosley et al. 2002; Arnould & Goriely 2003).

Supernova nucleosynthesis has been studied in great detail in the last decades and current supernova models are very successful in explaining the solar abundances not only of the elements up to iron, but also for a range of heavier nuclei produced in the weak s process, the νp process, and the γ pro-

cess (Fröhlich et al. 2006; Woosley & Heger 2007; Sukhbold et al. 2016; Pignatari et al. 2016; Travaglio et al. 2018; Prantzos et al. 2018; Wanajo et al. 2018; Curtis et al. 2019).

In addition to initiating the supernova explosions in the neutrino driven mechanism, neutrinos also affect the composition of the ejecta directly. By now, a range of extensive studies have been performed that also include the effects of neutrino induced reactions, summarized as the ν process. Electron neutrino and antineutrino captures as well as neutral-current spallation reactions, involving all neutrino species, have been shown to be able to contribute to the production of ^7Li , ^{11}B , ^{15}N , ^{19}F , ^{138}La , and ^{180}Ta (Woosley et al. 1990; Heger et al. 2005). Within ν -process studies, effects of MSW flavor oscillations (Yoshida et al. 2008) and collective oscillations (Wu et al. 2015) and the production of ^{92}Nb and ^{98}Tc (Cheoun et al. 2012) have also been explored.

Since neutrinos are expected to play a crucial role for successful supernova explosions, there is great interest in constraints on the neutrino emission characteristics. This has

been a major motivation to conceive and improve neutrino detectors that can provide insights into the supernova mechanism in case an event occurs close enough to earth (see Scholberg 2012, for a review). The ν process establishes a direct connection between the production of individual isotopes and supernova neutrinos. This allows in principle to constrain the neutrino spectra with nucleosynthesis arguments as demonstrated by Yoshida et al. (2005, 2006), even though uncertainties of nuclear and neutrino physics require such arguments to be taken with caution (Austin et al. 2011; Wu et al. 2015).

In addition to the uncertainties mentioned above, such constraints on the supernova neutrino energies derived from nucleosynthesis arguments suffer from two conceptual caveats: First of all, they are based on comparisons to the solar system composition, which is not the result of a single supernova explosion but involves contributions from a multitude of events over an incompletely known history of our galaxy. Therefore, large scale statistical sampling of models is necessary to draw conclusions. Another limiting aspect are the strong simplifications that are made in the modeling of the neutrino emission. In this paper we improve this description and quantify the impact of the latter aspect. The ν process has so far mostly been included in the same parametrization as originally suggested by Woosley et al. (1990), assuming neutrino luminosities that decrease exponentially with time as

$$L_\nu(t) = L_0 e^{-t/\tau_\nu} \quad (1)$$

and Fermi-Dirac spectra with constant average energies $\langle E_\nu \rangle$ for the different neutrino species. The values adopted for the average energies have been revised several times as supernova simulations have advanced, but the approach has remained the same (Heger et al. 2005; Yoshida et al. 2008; Banerjee et al. 2016; Sieverding et al. 2018).

This approach has been justified by the lack of more reliable data from either observations or from simulations on the details of the neutrino emission spectra and their time evolution. The field of supernova simulations has matured significantly during the last decades and, in particular, it has arrived at the point that calculations of different groups with different numerical methods obtain very similar results if they use the same initial conditions and assumptions (O'Connor et al. 2018). This motivates the present study of the impact of the details of the expected supernova neutrino signal on the ν process.

Recent years have brought a deeper understanding of the supernova mechanism, including in particular the role of multi-dimensional effects (Müller 2015; Janka et al. 2016; O'Connor & Couch 2018; Radice et al. 2018; Burrows et al. 2018) and while not all aspects of the supernova neutrino emission are quantitatively agreed upon, the main features have been understood on a qualitative level that even allows analytic models to achieve reasonable agreement with nu-

merical simulations (Janka 2001; Müller et al. 2016). Three major phases of neutrino emission from the core of a collapsing star can be distinguished:

1. First, there is a very luminous deleptonization outburst of electron neutrinos that emerges as the initial bounce shock dissociates nuclei into free protons and neutrons and thins out the material enough for it to become transparent to the neutrinos produced mostly by electron captures on free protons.
2. As the bounce shock stalls, accreting material sheds its gravitational binding energy by vigorous emission of all flavors of neutrinos produced mostly by thermal processes. During this phase the diffusive emission from the core is increased by a dynamic component that depends on the mass accretion rate and thus on the progenitor structure. The duration of this phase is determined by the conditions of shock revival and can be prolonged by multi-dimensional fluid flows.
3. Kelvin-Helmholtz cooling of the nascent neutron star is accompanied by strong neutrino emission for about 10 s. Due to the long duration the majority of the neutrinos are emitted during this phase, though at lower energies than in the previous phases.

In previous studies of the ν process (Woosley et al. 1990; Heger et al. 2005; Yoshida et al. 2008; Sieverding et al. 2018) it is assumed, that only the thermally produced neutrinos from the neutron star cooling phase are relevant for the nucleosynthesis. In the cooling phase (Phase 3), all neutrino flavors are produced equally and the total luminosity is distributed equally among the flavors. The ν process operates more efficiently at stellar radii where material is not heated to such large temperatures that thermonuclear reactions modify substantially the composition. Under these assumptions, the model-dependent time evolution of the neutrino luminosity and energy are of minor importance and the integrated neutrino emission properties such as the total energy emitted in neutrinos and an estimate for typical neutrino spectra are sufficient in order to estimate the nucleosynthesis. The total neutrino energy can, to some extent, be constrained by the difference of the gravitational binding energy of the stellar iron core and the final remnant under the assumption that all the neutrinos are produced during the proto-neutron star cooling. This leads to the commonly-used value of a total energy of $E_{\nu,\text{tot}} = 3 \times 10^{53}$ erg corresponding roughly to the gravitational binding energy of a neutron star (e.g. Cooperstein 1988).

In this paper, we test the validity of this approach by performing ν -process nucleosynthesis studies with 4 different treatments of the neutrino emission. In our **Approaches**

Table 1. Overview of the four different approaches applied in this manuscript for the description of the ν -process nucleosynthesis. The table lists how the time dependence of the average neutrino energies and pinching parameter has been treated individually for all neutrino species (ν_e , $\bar{\nu}_e$, ν_x , $\bar{\nu}_x$) based on the data from the simulation of [Mirizzi et al. \(2016\)](#). All approaches consider neutrino fluxes from the beginning of the nucleosynthesis calculations but use information from different neutrino emission phases. Only Approach 1a considers the full time dependence of the neutrino emission. Approaches 2 and 3 use Equation 1 with constant average neutrino energies. Approach 3 neglects the burst and accretion phases for the determination of the time-averaged energies. $\alpha = 2.3$ indicates that the spectra of Equation (4) are used with this constant value for α ^a.

Approaches	Neutrino emission phases					
	Neutrino burst		Accretion phase		Kelvin-Helmholtz cooling	
	$\langle E_\nu \rangle$	pinching (α)	$\langle E_\nu \rangle$	pinching (α)	$\langle E_\nu \rangle$	pinching (α)
1a*	t -dependent	t -dependent	t -dependent	t -dependent	t -dependent	t -dependent
1b	t -dependent	$\alpha = 2.3$	t -dependent	$\alpha = 2.3$	t -dependent	$\alpha = 2.3$
2**	t -independent	$\alpha = 2.3$	t -independent	$\alpha = 2.3$	t -independent	$\alpha = 2.3$
3	-	-	-	-	t -independent	$\alpha = 2.3$

^aEven if the analytical form of the $\alpha = 2.3$ distribution and of a Fermi-Dirac spectrum are different they are indistinguishable in practical numerical applications

* Full spectral information from neutrino radiation transport simulations including time dependent luminosities, average energies and pinching parameter

** Assumes the same time independent average energy for the three different phases, but all phases are taken into account for the determination of the that energy according to Equation (9)

1a and **1b**, we consider time-dependent neutrino luminosities and average energies for all neutrino species, taken from a supernova simulation. This study does not only take the proper time dependence of the neutrino emission into account, it also considers, for the first time, the impact of Phases 1 and 2 (burst and accretion, as defined above). **Approaches 1a** and **1b** differ in the treatment of the neutrino spectra. In **Approach 1a** we also account for pinched spectra, i.e., deviations of the neutrino emission spectra from a Fermi-Dirac spectrum with zero chemical potential (in the following referred to as FD spectra). In order to disentangle the effects of pinched neutrino spectra, **Approach 1b** assumes FD-like spectra for the emitted neutrinos, as this has been the case in previous studies of neutrino nucleosynthesis. **Approach 1a** represents our full improvement to neutrino nucleosynthesis, considering the time dependence of the neutrino emission and including pinched spectra. The calculations performed in **Approach 1a** are also confronted with two studies performed in analogy to previous studies, i.e., with constant average neutrino energies and assuming FD-like neutrino spectra. These two approaches differ in the way the time-average of the neutrino energies is determined. **Approach 2** is consistent with the first calculation, i.e., the average is performed over the complete neutrino emission spectrum, including Phases 1 and 2. Thus, it allows to study the sensitivity of the nucleosynthesis results to the time evolution of the neutrino emission. **Approach 3** more closely follows previous studies, by considering in the average only neutrinos emitted during the cooling phase. It neglects the

neutrino emission Phases 1 and 2 and thus allows to pin down their effect on the nucleosynthesis.

In Approaches 2 and 3 total energies $E_{\nu,\text{tot}}$ are obtained from the simulation for ν_e , $\bar{\nu}_e$ and the heavy flavors ν_x and $\bar{\nu}_x$ separately, but including on the one hand the whole duration of the emission (Approach 2) and on the other hand only the Kelvin-Helmholtz cooling phase (Approach 3). The parametrization of the neutrino luminosities is then adjusted to the total energies and the average energies of the various neutrino species are obtained as $\langle E_\nu \rangle = E_{\nu,\text{tot}}/N_{\nu,\text{tot}}$, such that the integrated number of emitted neutrinos $N_{\nu,\text{tot}}$ equals the included phases of the supernova simulation. With this definition of time-averaged energies the total number of neutrinos and the energy are the same in Approaches 1 and 2. Table 1 gives an overview of the four approaches used in this paper.

More details about the different Approaches and of our calculations are given in §2 together with a discussion of the simulation data we use. The impact on the nucleosynthesis is presented in §3 with further details on the role of pinched neutrino spectra in §4. Finally, the sensitivity to variations of the accretion time and the neutrino burst luminosity are explored in §5.

2. NEUTRINO SIGNAL FROM SUPERNOVA SIMULATIONS

In our ν -process calculations we combine a piston driven explosion model as in [Woosley & Weaver \(1995\)](#), tuned to produce an explosion energy of 1.2×10^{51} erg, with neutrino emission data from a numerical simulation (discussed in more detail below) and a large nuclear network. The neutrino emission is sensitive to the detailed dynamics of the

high density matter at the stellar core. As the ν process occurs at radii larger than 1,000 km, the neutrino emission processes and the propagation of the shock through the mantle can be treated as decoupled processes.

For the ν process we need to take into account neutrino-induced charged- and neutral-current reactions that affect the nuclear composition (Kolbe et al. 2003). In the charged-current reactions, the neutrino (antineutrino) transforms a neutron (proton) in the nucleus into a proton (neutron). At the supernova neutrino energies involved, this process can only occur for electron neutrinos and antineutrinos. It might, however, be accompanied by the emission of a single or multiple light particles (proton, neutron, α particle). Neutral-current reactions can be initiated by all neutrino flavors. For the ν process we are interested in neutrino-induced spallation reactions in which the neutrino excites the nucleus above (single or multiple) particle emission thresholds so that the excited nuclear level can decay by particle emission, changing the matter composition. The relevant neutrino-induced partial reaction cross sections are described in a two-step process, following Kolbe et al. (1992); Langanke et al. (1996); Balasi et al. (2015); Huther (2014). In the first step, the neutrino-induced nuclear excitation function is calculated. This step is usually performed within the framework of the Random Phase Approximation (RPA), but for selected nuclei these calculations are based on large-scale shell model calculations or on experimental data on Gamow-Teller strength functions (see Sieverding et al. 2018). The second step, i.e., the decay of the excited nuclear levels, is described within the statistical model, including also multi-particle emission channels (Huther 2014; Sieverding et al. 2018).

The neutrino-induced partial differential cross sections are incorporated into our nuclear reaction network, which evolves the abundances, $Y_i(t)$, of 1988 nuclear species connected by the thermonuclear reaction rates from the JINA REACLIB database (Cyburt et al. 2010) and β decays from the NUBASE compilation of experimentally determined values (Audi et al. 2017) where available and otherwise from the theoretical predictions by Möller et al. (2003). In the equations of the nuclear reaction network, the neutrino-nucleus reactions enter as additional terms in the form

$$\frac{\partial Y_i(t)}{\partial t} = \langle \sigma_\nu \rangle_{i,j}(t) \phi_\nu(t) Y_j(t), \quad (2)$$

with

$$\langle \sigma_\nu \rangle_{i,j}(t) = \int_0^\infty \sigma_{i,j}(E_\nu) n_\nu(E_\nu, t) dE_\nu, \quad (3)$$

where $\phi_\nu(t) = L_\nu(t)/[4\pi r^2(t) \langle E_\nu \rangle(t)]$ is the neutrino number flux at radius r and $\sigma_{i,j}(E_\nu)$ is the energy dependent neutrino-nucleus cross section. The indices j, i refer to the struck nucleus and the larger nuclear fragment in the final channel,

respectively, and $n_\nu(E_\nu, t)$ is the normalized neutrino spectrum at time t . Appropriate equations are included for the light particle produced (proton, neutron, α -particle) by the neutrino-induced reactions and for the struck nucleus where its abundance, Y_j , is decreased by the neutrino-nucleus reaction.

In our studies we use the neutrino-nucleus reaction cross sections of Sieverding et al. (2018), except for the reactions on ^4He and ^{12}C , which are taken from shell model calculations by Yoshida et al. (2008). The neutrino-induced reaction rates $\langle \sigma_\nu \rangle_{i,j}$ are then calculated with the appropriate neutrino emission data, considering time-dependent (Approaches 1a and 1b) or constant (Approaches 2 and 3) average neutrino energies.

Following Keil et al. (2003) and Tamborra et al. (2012), the instantaneous normalized neutrino spectra are represented by a quasithermal distribution:

$$n_\nu(E) \equiv \left(\frac{\alpha + 1}{\langle E \rangle} \right)^{\alpha+1} \frac{E^\alpha}{\Gamma(\alpha + 1)} \exp\left(-\frac{(\alpha + 1)E}{\langle E \rangle}\right), \quad (4)$$

with the Gamma function Γ . The parameter α can be obtained from the second moment of the neutrino spectra:

$$\frac{\langle E_\nu^2 \rangle}{\langle E_\nu \rangle^2} = \frac{\alpha + 2}{\alpha + 1}. \quad (5)$$

A value of $\alpha = 2.0$ corresponds to the limit of a Maxwell-Boltzmann distribution, whereas $\alpha = 2.3$ very closely matches a Fermi-Dirac spectrum with zero chemical potential:

$$n_{\text{FD}}(E) = \frac{2}{3\zeta(3)T_\nu^3} \frac{E^2}{\exp(E/T_\nu) + 1}, \quad (6)$$

with the neutrino temperature, T_ν , related to the average neutrino energy $T_\nu = 180\zeta(3)\langle E_\nu \rangle/(7\pi^4)$, where ζ is the Riemann zeta-function. Values $\alpha > 2.3$ account for increasingly pinched spectra, whereas $\alpha < 2.3$ corresponds to an “anti-pinching” in which high energy neutrinos are more likely to be encountered than in the equilibrium Fermi-Dirac distribution. It has been found already by early calculations (Janka & Hillebrandt 1989; Giovanoni et al. 1989; Myra & Burrows 1990) that the neutrino spectra emitted from a supernova explosion tend to be pinched and also modern calculations (Keil et al. 2003; Tamborra et al. 2012; Mirizzi et al. 2016) show the same trend (see Figure 1). With relevance to neutrino nucleosynthesis we note that, in general, pinched spectra result in reduced folded neutrino-nucleus cross sections, $\langle \sigma_\nu \rangle$, compared to those obtained with FD spectra, as the number of high-energy neutrinos is reduced, while on the other hand anti-pinched spectra yield larger cross sections. Neutrino-nucleus cross sections for different forms of neutrino spectra are given in (Kolbe et al. 1992; Langanke & Kolbe 2001).

We use neutrino luminosities and spectra from a one-dimensional, artificially exploded supernova simulation (Mirizzi et al. 2016). It included a detailed treatment of neutrino transport with a two-moment scheme and a variable Eddington factor closure derived from a model-Boltzmann equation (Rampp & Janka 2002), which constitutes an efficient numerical method to solve the integro-differential transport problem and gives results in good agreement with a direct solution of the Boltzmann equations (Liebendörfer et al. 2005).

This model has also been used by Bartl et al. (2016) to study the effects of an improved treatment of nucleon-nucleon bremsstrahlung on the proto-neutron star cooling phase. We remark that, at this point, we have to resort to artificially triggered one-dimensional supernova explosions for our ν -process studies because self-consistent 3D models are computationally very expensive and are therefore usually not run long enough to cover the whole proto-neutron star (PNS) cooling phase which is important for the ν process. The one-dimensional simulation for a $27 M_\odot$ progenitor used here includes effects of PNS convection treated with a mixing-length description. It is suitable for our purposes because it exhibits all the relevant features of the neutrino signal that are qualitatively also found in self-consistent multi-dimensional models (Mirizzi et al. 2016), and we consistently combine it with the $27 M_\odot$ progenitor model from Woosley & Heger (2007), from which we take the pre-supernova abundances and structure.

Figure 1 shows the neutrino luminosities and spectral properties as obtained in the simulation of Mirizzi et al. (2016). In particular, the figure distinguishes the three different emission phases as defined above. The two upper panels show the luminosities and the average neutrino energies, while the bottom panel shows the α parameter that characterizes the deviation from a FD spectrum. We note that the electron neutrino spectra are strongly pinched during the burst phase. This is related to the fact that the electron neutrinos with higher energies are affected by charged-current reactions even after ν_e -neutrinos with average energies are decoupled from matter (Giovanoni et al. 1989). During the accretion phase there is a relatively strong variation in the neutrino spectral forms, including short periods of anti-pinched spectra for ν_e and ν_x . During the cooling phase, the ν_x spectrum closely resembles a FD spectrum, while ν_e and $\bar{\nu}_e$ spectra are slightly pinched. $\bar{\nu}_x$ behave very similar to ν_x as shown by Mirizzi et al. (2016) and are omitted in Figure 1.

Our approach improves previous ν -process studies in four important aspects: (i) It considers the electron neutrino burst (Phase 1) which occurs during the first 10 ms after bounce and is associated with the shock breakout from the neutrino trapping regime (e.g. Janka et al. 2007). The burst alone contains 5 % of the total energy that is emitted in electron neutrinos. The burst phase was not considered in previous

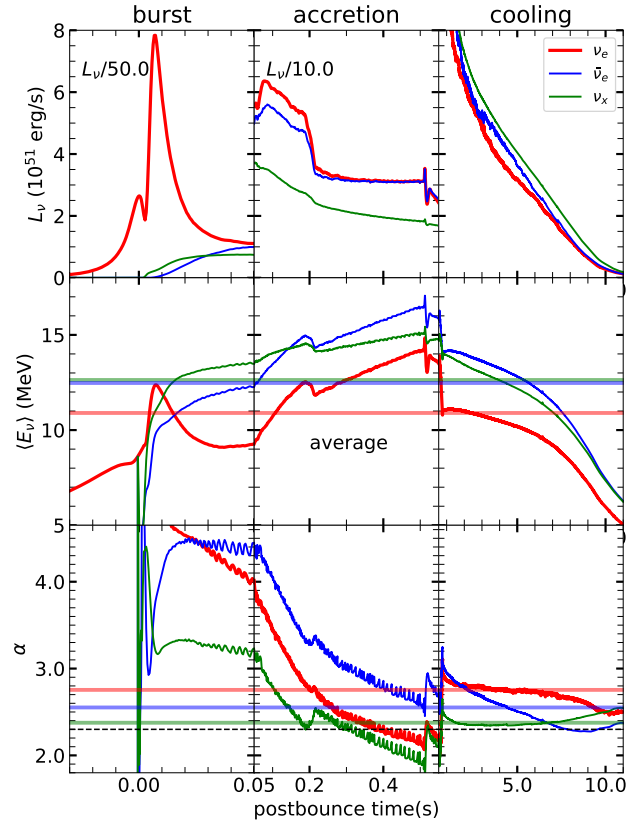


Figure 1. Time evolution of neutrino luminosities and energies from a one-dimensional, artificially triggered supernova simulation (Mirizzi et al. 2016). The calculation uses the SFHo equation of state (Steiner et al. 2013). The top panels show the luminosities and the middle panels the average neutrino energies. The horizontal lines in the middle panel indicate the representative energies as defined by Equation (9). During the accretion period, the actual neutrino energies are substantially higher than the representative values. The bottom panel shows the value of α as defined in Equation (4) that describes the pinching of the neutrino spectra.

studies. (ii) Our study includes the prolonged phase of accretion (Phase 2) as material falls through the stalled shock. In Mirizzi et al. (2016), the explosion has been artificially initiated at 0.5 s after the bounce, effectively ending the accretion phase, since in a one-dimensional model matter cannot pass around the expanding material. We note that the duration of the accretion phase is somewhat uncertain and that the longer this period lasts, the more effectively neutrinos can contribute to the nucleosynthesis. We study the impact of the length of the accretion phase on the neutrino nucleosynthesis in §5. The accretion phase has not been included in previous studies. (iii) Rather than using the parametric form of Equation (1), we consider the time-dependence of the luminosities for the individual neutrino species as given by Mirizzi et al. (2016). We note, however, that the luminosities during the

cooling phase, which starts around 500 ms after bounce, are relatively well described by an exponential decline $L_\nu \propto e^{-t/\tau}$ with $\tau = 3$ s, as adopted in previous studies (and in our approaches 2 and 3). (iv) Since the supernova simulation treats the neutrino transport with multiple energy groups, it does not only contain information about neutrino fluxes and the average energies but it also provides information about the spectral shape, expressed in terms of $\langle E^2 \rangle$, that is related to α by Equation (4)

Table 2. Cross sections for the reactions for which the spectral shape was taken into account

Reaction	Cross section in 10^{-42} cm^2		
	$\alpha = 2.3$	$\alpha = 2.5$	$\alpha = 2.8$
$^4\text{He}(\nu, \nu' p)^3\text{He}$	1.00×10^{-2}	8.31×10^{-3}	6.38×10^{-3}
$^4\text{He}(\nu, \nu' n)^3\text{He}$	9.26×10^{-3}	7.68×10^{-3}	5.88×10^{-3}
$^{12}\text{C}(\nu, \nu' p)^{11}\text{B}$	3.44×10^{-2}	2.94×10^{-2}	2.35×10^{-2}
$^{12}\text{C}(\nu, \nu' n)^{11}\text{C}$	9.86×10^{-3}	8.30×10^{-3}	6.51×10^{-3}
$^{16}\text{O}(\nu, \nu' p)^{15}\text{N}$	6.01×10^{-2}	5.14×10^{-2}	4.14×10^{-2}
$^{16}\text{O}(\nu, \nu' n)^{15}\text{O}$	1.51×10^{-2}	1.28×10^{-2}	1.01×10^{-2}
$^{16}\text{O}(\nu, \nu' \alpha p)^{11}\text{B}$	1.22×10^{-5}	9.21×10^{-6}	6.18×10^{-6}
$^{16}\text{O}(\nu, \nu' an)^{11}\text{C}$	2.73×10^{-5}	2.08×10^{-5}	1.42×10^{-5}
$^{20}\text{Ne}(\nu, \nu' p)^{19}\text{F}$	3.15×10^{-3}	2.66×10^{-3}	2.11×10^{-3}
$^{20}\text{Ne}(\nu, \nu' n)^{19}\text{Ne}$	8.29×10^{-2}	7.22×10^{-2}	5.94×10^{-2}
$^{12}\text{C}(\nu_e, e^- p)^{11}\text{C}$	8.58×10^{-2}	7.12×10^{-2}	5.47×10^{-2}
$^{12}\text{C}(\bar{\nu}_e, e^+ n)^{11}\text{B}$	3.20×10^{-4}	2.59×10^{-4}	1.91×10^{-4}
$^{138}\text{Ba}(\nu_e, e^-)^{138}\text{La}$	6.36×10^1	6.20×10^1	5.98×10^1
$^{138}\text{Ba}(\nu_e, e^- n)^{137}\text{La}$	6.22×10^1	5.82×10^1	5.30×10^1
$^{180}\text{Hf}(\nu_e, e^-)^{180}\text{Ta}$	1.16×10^2	1.13×10^2	1.10×10^2
$^{180}\text{Hf}(\nu_e, e^- n)^{179}\text{Ta}$	7.61×10^1	7.22×10^1	6.71×10^1

NOTE—Cross sections have been folded with spectra as in Equation (4) with different values of α and $\langle E_\nu \rangle = 12.6$ MeV.

Including the effects of the spectral shape requires to fold the cross section with the spectrum according to Equation (3) for each time step of the calculation. This is computationally challenging. Therefore, we include the full spectral shape only for a limited set of neutrino-nucleus reactions that are the most important. The reactions are listed in Table 2 and include the main reactions for the production of ^7Li , ^{11}B , ^{15}N , ^{19}F , ^{138}La and ^{180}Ta . The production of ^7Li and ^{11}B in the He shell proceeds via the reactions $^3\text{He}(\alpha, \gamma)^7\text{Be}(\alpha, \gamma)^{11}\text{C}$ and $^3\text{H}(\alpha, \gamma)^7\text{Li}(\alpha, \gamma)^{11}\text{B}$, initiated by neutrino-induced reactions on ^4He to provide ^3He and ^3H , which are not produced significantly by thermal photons because the matter temperature is too low. For all other reactions we assume a Fermi-Dirac spectrum $n_{\text{FD}}(E_\nu)$ and interpolate the cross sections from a set of values calculated as a function of the spectral average energy $\langle E_\nu \rangle(t)$. In this way we account for the evo-

lution of the neutrino spectra with time as predicted by the simulation.

In Table 2 we compare the folded cross sections, $\langle \sigma_\nu \rangle$, for a FD-like spectrum ($\alpha = 2.3$) with those obtained with pinched spectra ($\alpha = 2.5$ and 2.8) as they occur for electron neutrinos and electron antineutrinos in the cooling phase and for ν_x neutrinos in the accretion phase, assuming a typical average energy $\langle E_\nu \rangle = 12.6$ MeV. The cross sections decrease with increasing value of α , i.e. pinching, but the effect of the pinched spectra on the cross sections depends also quite sensitively on the reaction thresholds. As neutral-current induced spallation reactions have in general large particle emission thresholds, the effect of pinching is sizable here, as can be seen for the neutral-current reactions on ^4He , ^{12}C and on ^{20}Ne . However, neutral-current reactions are mainly induced by ν_x neutrinos during the cooling phase and their spectra in this phase resemble FD spectra relatively closely. Hence, the consideration of pinched spectra, as performed here for the first time, should not have too strong an impact on the neutrino nucleosynthesis yields of nuclides which are produced by neutral-current reactions. On the other hand, charged-current reactions have smaller threshold energies, which reduces the impact of the pinched spectra. The results obtained for the (ν_e, e^-) reactions on ^{138}Ba and ^{180}Hf are examples. In both cases the cross section is reduced by a few percent, comparing the cross sections for the FD-like spectrum ($\alpha = 2.3$) to the values obtained with the pinched spectrum with $\alpha = 2.8$. The effect is somewhat larger, if one compares charged-current reactions with emission of particles (neutrons for the cases of ^{138}Ba and ^{180}Hf), because an additional threshold has to be overcome. The effect is more significant for the $(\nu_e, e^- p)$ and $(\bar{\nu}_e, e^+ n)$ reaction cross sections on ^{12}C due to the relatively large threshold energies involved. The effects on the nucleosynthesis yields are explored in more detail in §4.

We adjust the time of the neutrino data such that the peak in the electron neutrino luminosity coincides with the time the piston is launched. We assume that the neutrinos travel at the speed of light and therefore the arrival of the neutrino signal is slightly delayed for mass shells at larger radii.

The result of our Approach 1a, which uses the fully time-dependent neutrino data from the simulation, is compared to Approaches 2 and 3 that use approximations similar to previous neutrino nucleosynthesis calculations and also assume a constant value of $\alpha = 2.3$ for the reactions listed in table 2. In these models average energies are constant and the neutrino luminosity is described by Equation (1). L_0 is fixed by requiring that the time integrated luminosity gives the same value of the total energy emitted as neutrinos,

$$E_{\nu, \text{tot}} = \int_{t_0}^{t_{\text{end}}} L_\nu(t) dt, \quad (7)$$

as obtained with the numerical values of $L_\nu(t)$ provided by the simulation, which covers the time from $t_0 = -0.3$ s (before bounce) until $t_{\text{end}} = 11.2$ s after bounce.

Based on the simulation, the total energy emitted as neutrinos, $E_{\nu,\text{tot}}$, is 3.49×10^{53} erg. The distribution among the neutrino flavors is almost equal. We find that ν_e contribute 0.62×10^{53} erg, $\bar{\nu}_e$ amount to 0.59×10^{53} erg and the heavy flavors μ and τ give 2.27×10^{53} erg for neutrinos and antineutrinos together. In our Approach 2, the entire neutrino signal is considered to calculate $E_{\nu,\text{tot}}$. Whereas Approach 3 is similar to previous studies in that it takes into account only the PNS cooling phase starting at $t_0 = 500$ ms after bounce, when the explosion was triggered. This results in a total energy emitted as neutrinos of 2.53×10^{53} erg, of which 0.37×10^{53} erg are from ν_e , 0.40×10^{53} erg are from $\bar{\nu}_e$ and the remainder from the heavy flavor neutrinos.

A second integral quantity of the neutrino signal is the total number of emitted neutrinos, that we calculate from the simulation data as

$$N_{\nu,\text{tot}} = \int_{t_0}^{t_{\text{end}}} \frac{L_\nu(t)}{\langle E_\nu \rangle(t)} dt. \quad (8)$$

Again, in our Approach 2, the entire neutrino signal is considered to calculate $N_{\nu,\text{tot}}$, while Approach 3 limits the integration to the cooling phase, i.e., $t_0 = 0.5$ s.

With different values of $E_{\nu,\text{tot}}$ and $N_{\nu,\text{tot}}$ Approaches 2 and 3 also use different values of the constant, time-averaged neutrino energies calculated as

$$\langle E_\nu \rangle = \frac{E_{\nu,\text{tot}}}{N_{\nu,\text{tot}}} \quad (9)$$

For Approach 2 we obtain $\langle E_{\nu_e} \rangle = 10.9$ MeV, $\langle E_{\bar{\nu}_e} \rangle = 12.6$ MeV, $\langle E_{\nu_x} \rangle = 11.7$ MeV and $\langle E_{\bar{\nu}_x} \rangle = 12.6$ MeV. These are effectively the same average values as the set of “low” neutrino energies discussed and adopted in Sieverding et al. (2018) except for the electron neutrinos.

For Approach 3 we find $\langle E_{\nu_e} \rangle = 10.6$ MeV, $\langle E_{\bar{\nu}_e} \rangle = 13.3$ MeV, $\langle E_{\nu_x} \rangle = 12.5$ MeV and $\langle E_{\bar{\nu}_x} \rangle = 13.3$ MeV, relatively close to the values used by Sieverding et al. (2018), i.e., $\langle E_{\nu_e} \rangle = 8.8$ MeV, $\langle E_{\bar{\nu}_e} \rangle = \langle E_{\nu_x} \rangle = \langle E_{\bar{\nu}_x} \rangle = 12.6$ MeV.

In Approaches 2 and 3 we use FD-like neutrino spectra with a constant (time-independent) average energy, which still differs for ν_e , $\bar{\nu}_e$, ν_x and $\bar{\nu}_x$ neutrinos. This ansatz is equivalent to the assumption of constant time-independent average energies for the different neutrino species.

Nucleosynthesis studies published prior to 2018 used neutrino emission spectra with noticeably higher energies, as they were appropriate at the time they were performed, e.g., $\langle E_{\nu_e} \rangle = 12.6$ MeV, $\langle E_{\bar{\nu}_e} \rangle = 15.8$ MeV, $\langle E_{\nu_x} \rangle = \langle E_{\bar{\nu}_x} \rangle = 18.9$ MeV in Heger et al. (2005).

3. IMPACT OF THE IMPROVED DESCRIPTION OF THE NEUTRINO EMISSION ON THE ν PROCESS

In this section we report on the results which we obtain in our nucleosynthesis studies for a $27 M_\odot$ progenitor star using the improved neutrino emission description based on the supernova simulation of Mirizzi et al. (2016) and defined in the previous section (Approaches 1a and 1b). Note that Approach 1a includes also effects of the pinching of neutrino spectra which are discussed in detail in §4. The $27 M_\odot$ progenitor star used here does not reflect the full picture of neutrino nucleosynthesis. It has some peculiarities which are, for example, not found in lower mass progenitors (Sieverding et al. 2018) and which we will address below. Our goal here is to explore the impact of the various improvements which we consider in the description of the neutrino emission signal. To this end, the results of our Approach 1b are compared to calculations in which these improvements were either treated approximately (time-independent average neutrino energies, Approach 2) or partly ignored (no consideration of the burst and accretion phases and time-independent average neutrino energies, Approach 3). As stated above, Approach 3 reflects the spirit of previous studies of neutrino nucleosynthesis.

Table 3. Production factors

Nucleus	Appr. 1a $\alpha = \alpha(t)$	Appr. 1b $\alpha = 2.3$	Appr. 2 $\alpha = 2.3$	Appr. 3 $\alpha = 2.3$	literature FD
^7Li	0.04	0.04	0.03	0.02	0.02
^{11}B	0.30	0.31	0.28	0.18	0.13
^{15}N	0.06	0.05	0.05	0.04	0.04
^{19}F	0.12	0.12	0.11	0.10	0.10
^{138}La	0.69	0.74	0.66	0.41	0.44
$^{180}\text{Ta}^m$	1.32	1.33	1.27	1.09	1.11

NOTE—Production factors are normalized to ^{16}O , see Equation (10), comparing the different approaches for the description of the neutrino irradiation discussed in the text for the $27 M_\odot$ model. Only Approach 1a takes the spectral shape described by $\alpha(t)$ into account and is discussed in §4. The column labeled “literature” gives the results of Sieverding et al. (2018) who assumed Fermi-Dirac spectra with vanishing chemical potential for the neutrinos. Results given for $^{180}\text{Ta}^m$ assume that 35% of the produced ^{180}Ta at 200 s after bounce survive in the isomeric state $^{180}\text{Ta}^m$.

The results of our nucleosynthesis studies are summarized in Table 3. We list production factors, P , normalized to ^{16}O , i.e.,

$$P = [X_*(A, Z)/X_\odot(A, Z)]/[X_*(^{16}\text{O})/X_\odot(^{16}\text{O})], \quad (10)$$

with solar mass fractions X_\odot from Lodders (2003) and the stellar mass fractions X_* obtained from our calculations.

More recent evaluations of the solar system abundances are available (Lodders et al. 2009; Asplund et al. 2009), but for consistency within this paper we use the same values that were assumed for the initial composition of the progenitor model. The ground state of ^{180}Ta has too short a β -decay half-life (8.2 hours) to contribute to the abundance in the solar system. Only the long-lived isomeric state $^{180}\text{Ta}^m$ with a halflife of $\sim 10^{15}$ yr is still present. In our calculations, we do not follow the ground and isomeric states separately, but rather determine the population of the isomeric state in our reaction network by adopting the estimate of Mohr et al. (2007) and Hayakawa et al. (2010) that 35%–39% of the total ^{180}Ta abundance survives in the isomeric state. The yields and production factors for $^{180}\text{Ta}^m$ shown in Table 3 are 35% of the calculated ^{180}Ta yields.

Before entering the detailed discussion of the effect of our improved treatment of the neutrino emission, we note that, qualitatively, our calculations using the full neutrino emission signal (Approaches 1a and 1b) confirm the general conclusions drawn in Sieverding et al. (2018) for the neutrino-induced production of the nuclides ^7Li , ^{11}B , ^{15}N , ^{19}F , ^{138}La , and ^{180}Ta . In agreement with previous studies (Woosley et al. 1990; Heger et al. 2005; Sieverding et al. 2018), using an extensive nuclear network, we do not find evidence for other nuclides being significantly produced by the ν process. Comparing our results with Approaches 1a and 1b to the more approximate Approaches 2 and 3, however, we find some significant differences that demonstrate the importance of the improved treatment of the neutrino signal. Table 3 shows that differences are largest between Approach 1b and Approach 3. For Approach 3, which is in the spirit of the previous studies, the yields are noticeably less than in our improved study with differences ranging between 16% for ^{19}F to 50% for ^7Li . This shows that the neutrino emission from the burst and accretion phases needs to be included. With Approach 2, considering all three neutrino emission phases, the reduction is noticeably smaller, but in Approach 2 we have ignored the time dependence of the average neutrino energies by using constant average energies for the individual neutrino species. With this approach we still find smaller nucleosynthesis yields for the ν -process nuclei compared to Approach 1a but the reduction is on the level of a few percent for all species. This difference is due to the energy dependence that enters the neutrino-nucleus cross section via the phase space factor. This additional energy factor favors the contribution arising from neutrino energies higher than average relative to those lower than average and is explained in more detail below. We note that the yields calculated in our Approach 3 agree quite well with those presented by Sieverding et al. (2018) using the same progenitor and explosion model. As stated above, Approach 3 is performed using the same general assumptions in the description of the neu-

trino emission signal and the remaining differences between the two calculations can be traced back to two compensating effects: The time-integrated neutrino luminosity assumed by Sieverding et al. (2018), is slightly larger than that calculated in Approach 3 (3×10^{53} erg compared to 2.53×10^{53} erg, respectively). This reduces the yields with our Approach 3. On the other hand, the average energies of the various neutrino species are slightly smaller in Sieverding et al. (2018) than in our Approach 3, increasing our yields. Our Approach 3 results in significantly lower yields for the ν -process isotopes than obtained in earlier studies (e.g., Woosley et al. 1990; Heger et al. 2005; Yoshida et al. 2005, 2008), who assumed neutrino spectra with noticeably larger average energies.

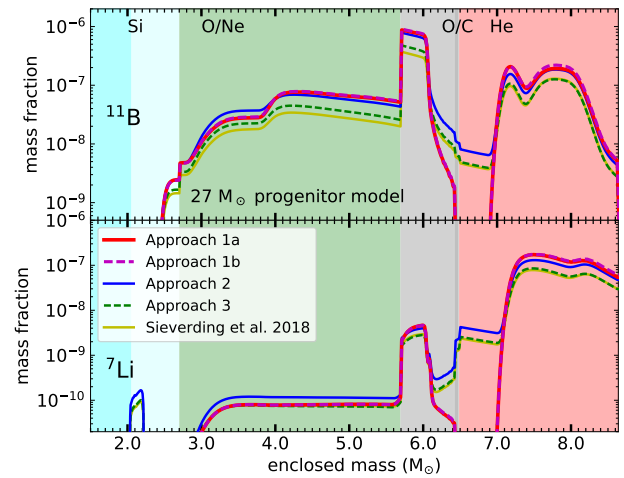


Figure 2. Mass fraction profiles of ^{11}B (upper panel) and ^7Li (lower panel) for the $27 M_{\odot}$ model using different descriptions of the neutrino spectra and time evolution. The mass fractions are evaluated after nuclear β decays of radioactive isotopes and the background colors indicate the compositional shells as indicated at the top. Results for our Approaches 1a and 1b are almost identical. Approach 2 shows a reduced mass fraction. For comparison, the results using the low neutrino energies from Sieverding et al. (2018), which are similar to our Approach 3, are also shown.

In the following, we discuss in detail where in the star the neutrino nucleosynthesis occurs and which differences result from including the early phases of neutrino emission and the time dependence of the average neutrino energies in Approaches 1a and 1b.

Figure 2 shows the mass fraction profiles of the light nuclides ^{11}B and ^7Li as obtained in the nucleosynthesis studies with our different approaches (see Table 1 for an overview of the approaches). Additionally, we give the results for the same stellar model presented by Sieverding et al. (2018), which, as discussed above, are close to those obtained in our Approach 3. Both nuclides are produced in the ν process by the reaction chains $^3\text{H}(\alpha, \gamma)^7\text{Li}(\alpha, \gamma)^{11}\text{B}$ and $^3\text{He}(\alpha, \gamma)^7\text{Be}(\alpha, \gamma)^{11}\text{C}$ following the neutrino-induced reac-

tions on ^4He that produce ^3He and ^3H . ^{11}C is radioactive and decays to ^{11}B with a halflife of 20 min. An important contribution to ^{11}B also comes from the O/C shell in which neutrino-induced spallation of ^{12}C produces ^{11}C and ^{11}B directly. A detailed discussion can also be found in Sieverding et al. (2018). Due to the inclusion of the burst and accretion phases, the electron neutrinos have a higher average energy in our Approach 2 compared to Approach 3 and to the values adopted by Sieverding et al. (2018). As a consequence, the production of ^{11}B in the C shell is increased, because charged-current reactions contribute almost half to the ^{11}B synthesis in this layer. In the He shell, ^{11}B is produced from the spallation products of neutral-current reactions on ^4He . As the average energies of ν_x , $\bar{\nu}_x$ and $\bar{\nu}_e$ are almost the same in our Approach 3 and the study of Sieverding et al. (2018) the neutral-current induced reaction chain produces essentially the same mass fraction of ^{11}B in the He shell. Approach 2, which also uses similar average energies, but a higher luminosity because it includes the early phases of neutrino emission, leads to a slightly larger ^{11}B abundance in the He shell. The mass fractions obtained in our Approaches 1a and 1b are very similar to each other, showing that the spectral shape has little impact on the production of these nuclei as discussed in more detail in §4. In both cases using the time-dependent neutrino energies, however, the mass fractions turn out to be larger in the He and C shells than found in Approaches 2 and 3. The production of ^7Li in the He shell stems to a large fraction from ν_e -induced reactions and, for the same reasons as for ^{11}B , we observe an increased mass fraction in our Approach 2 compared to Approach 3 and the results of Sieverding et al. (2018). A large fraction of ^7Li is first produced as ^7Be , started by the $^4\text{He}(\nu_e, e^- p)^3\text{He}$ and $^3\text{H}(\nu_e, e^-)^3\text{He}$ reactions followed by an α capture. Similar to ^{11}B , our Approaches 1a and 1b lead to a larger ^7Li mass fraction than the other calculations.

Using the time-dependent neutrino emission data in Approaches 1a and 1b increases the total production of ^7Li and ^{11}B , but the local mass fractions do not increase in all regions of the star. The mass fractions of ^{11}B and ^7Li in the outer C shell and at the base of the He shell at a mass coordinate of around $6.5 M_\odot$ are lower for the calculations with the time-dependent neutrino energies than in the other cases (see Figure 2). Around mass coordinate $3.2 M_\odot$, in the inner O/Ne shell our Approaches 1a and 1b also lead to an decrease of the mass fractions compared to Approach 2. These differences do not affect the total yields noticeably because the mass fractions in these regions are low compared to those in the He shell. Even though the total energy emitted in neutrinos, as defined by Equation (7), and the number of neutrinos, as defined by Equation (8), already give a good characterization of the neutrino emission for the ν process, as can be seen from the similar production factors of Approaches 1a/b

and 2 in Table 3, there are subtle effects that cannot be captured by an averaged approach that reproduces the same time-integrated energy and number of neutrinos.

To explain these subtle differences, we note that the results of the ν process are a competition of neutrino-induced reactions on one hand and the effect of the shock on the other. Both depend on the location in the star where the competition occurs. In general, at a smaller radius the shock induces higher temperatures, at which charged particle reactions run noticeably faster. Hence, the effectiveness of shock-initiated nucleosynthesis is increased, but still depends on the available seed-nuclei. The radius defines also the arrival time of the shock and which part of the neutrino emission signal acts before arrival of the shock and which after. The latter point is particularly important to explain the differences in the neutrino nucleosynthesis yields between our Approaches 1 and 2, i.e., whether we use the time-dependent spectra or replace them by spectra with a constant average energy. Supernova simulations indicate that the average energy of the emitted neutrinos decreases with time. Taking this into account in our Approaches 1a and 1b, late neutrinos, emitted after a few seconds, have spectra shifted to energies lower than those assumed in Approach 2. Thus, in our Approaches 1a and 1b, neutrino-induced reactions are less effective in rebuilding the abundances if the shock passage occurred only after a few seconds.

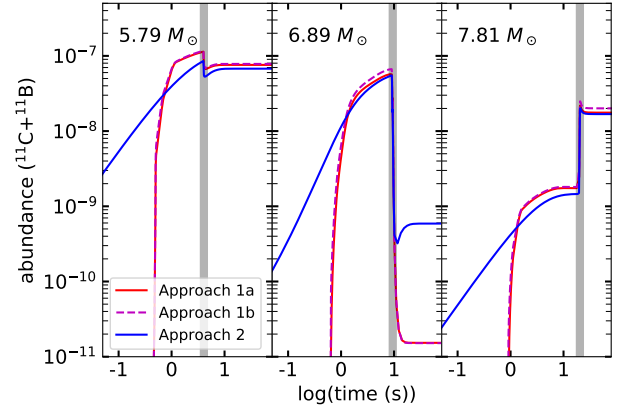


Figure 3. Evolution of the combined abundances of ^{11}B and ^{11}C for three selected mass zones, corresponding to the O/C shell, the lower He shell and the middle of the He shell, where the production is the most efficient. The corresponding mass coordinate is indicated in each panel. The abundance evolution for Approaches 1a and 1b, which both use the time-dependent neutrino energies and luminosities are shown in comparison to our Approach 2 which uses time-averaged constant values for the neutrino energies. Approach 1b and Approach 2 both use fixed values of $\alpha = 2.3$, whereas Approach 1a uses $\alpha(t)$ based on the supernova simulation. The shaded vertical line indicates the time when the supernova shock reaches the mass shell.

Our general conclusions are supported by Figure 3, which compares the abundance evolution of ^{11}B as a function of time for our Approaches 1a and 1b to Approach 2. The evolution is almost identical for Approaches 1a and 1b. This shows that the effects of the pinched spectra are much smaller than the effects of including the time-dependence of the neutrino energies, which is neglected in Approach 2 and leads to noticeable differences in the abundance evolution. We have depicted three locations in the star, moving outwards from the left panel to the right panel. The left panel shows the evolution in the O/C shell, where ^{11}B is made mostly as ^{11}C by the $^{12}\text{C}(\nu, \nu' n)$ reaction. Using the time-dependent signal (Approaches 1a and 1b), the production sets in later, but, due to the higher energy, the production quickly exceeds the case for the constant average neutrino energy¹. In the O/C shell, the supernova shock reduces the abundance only slightly, because only a few α particles are available for charged-particle reactions showing the importance of the composition. The shock passage takes place around $t = 4$ s and matter temperatures reach up to 1 GK. For both approaches, the neutrino flux is still substantial after the shock has passed and the abundances recover from the reduction caused by charged particle reactions initiated by the shock. This recovery is slightly stronger in Approach 2 than in Approach 1b, because the spectra of the late time neutrinos have smaller average energies than the constant value adopted in Approach 2. The middle panel depicts the situation close to the base of the He shell. Here, the shock arrives at about $t = 10$ s and reaches a temperature of 0.5 GK. In the He shell, α particles are readily available and the shock destroys most of the ^{11}B produced before its arrival. At $t > 10$ s the neutrino flux is already too low to recover the ^{11}B abundance after the passage of the shock. Moreover, at such late times, the time-dependent spectra used in Approaches 1a and 1b are noticeably shifted to lower average energies compared to those adopted in Approach 2. Thus, Approach 2 yields a higher final ^{11}B abundance than Approaches 1a and 1b at this location, as in Figure 2. In either case, the final abundances are, however, quite small and do not contribute noticeably to the total ^{11}B yield. The right panel of Figure 3 shows the abundance evolution further out in the He shell. The shock arrives after about $t = 20$ s and reaches a maximum temperature of 0.3 GK. This temperature is too low to destroy ^{11}B or ^{11}C by α reactions, but is still high enough to initiate the $^{7}\text{Be}(\alpha, \gamma)$ and $^{7}\text{Li}(\alpha, \gamma)$ reactions to produce additional ^{11}B . This production depends also on the availability of ^{7}Li and ^{7}Be at the time when the shock arrives. Their abundances are slightly higher in Approaches 1a and 1b than in Approach 2. In both approaches, the neutrino flux after passage of the shock is al-

ready too small to further change the ^{11}B abundance. At all three locations depicted in Figure 3 we note that the pinched spectra lead to a slight and systematic reduction of the ^{11}B abundance in calculations with Approach 1a compared to Approach 1b, which assumes $\alpha = 2.3$ throughout. These effects are discussed in more detail in §4.

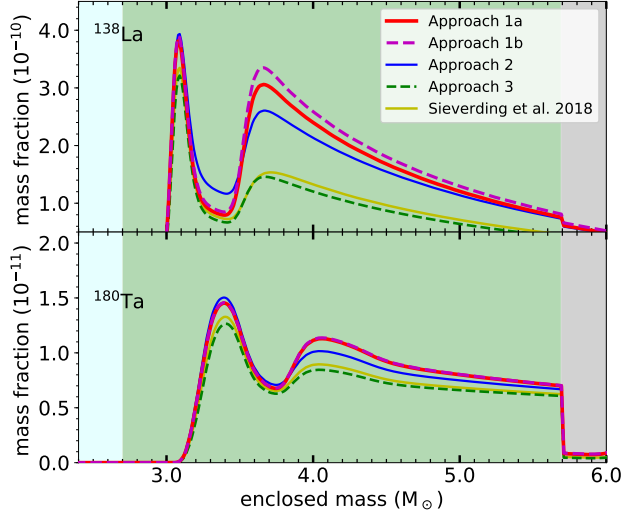


Figure 4. Same as Figure 2 but for ^{138}La and ^{180}Ta from the 27 M_\odot model comparing Approaches 1a and 1b to Approach 2. With the full neutrino signal used in Approaches 1a and 1b the mass fraction of ^{138}La is significantly increased compared to the approximation of Approach 2. Approach 3 results in even lower mass fractions very similar to Sieverding et al. (2018)

Figure 4 shows the mass fraction profiles for ^{138}La and ^{180}Ta in the 27 M_\odot star for five different treatments of the neutrino emission. Neutrino nucleosynthesis produces both nuclides mainly in the O/Ne shell by the charged-current reactions $^{138}\text{Ba}(\nu_e, e^-)$ and $^{180}\text{Hf}(\nu_e, e^-)$, respectively. The seed nuclides, ^{138}Ba and ^{180}Hf , which are noticeably more abundant, stem from the initial composition of the progenitor star modified by the γ process operating prior to the explosion (see Sieverding et al. 2018). The effect of the shock on the ^{138}La and ^{180}Ta yields results mainly from a competition of photodissociation, mostly (γ, n) , and (re-)capture of emitted neutrons. The matter temperature reached in the O/Ne shell is too low to initiate charged particle reactions on the two nuclides due to their high atomic numbers (Sieverding et al. 2018). The effect of photodissociation suggests to distinguish three different regions in the shell. In the outer shell, the temperatures are low and photodissociation does not play an important role. In this region, ^{138}La and ^{180}Ta are then almost unaffected by the supernova shock and the charged-current reactions induced by the entire ν_e signal add to the final yields. As discussed above, due to the energy dependence of the phase space factors early neutrinos with aver-

¹ The same early behavior before shock arrival is found also for the other two mass cells, shown in the middle and right panels.

age energies higher than the time-average can already in a short time exceed the production induced by neutrinos with the constant, time-averaged value for the energies. As a consequence, Approaches 1a and 1b give larger mass fractions than Approach 2. Approach 3 and the calculation by Sieverding et al. (2018) result in lower mass fractions due to lower average energies and lower luminosities. In this region the suppression of the production due to the pinched spectra with Approach 1a compared to 1b is most noticeable. Closer to the bottom of the O/Ne shell, the mass fractions show a minimum. In this region temperatures are sufficiently high during the shock passage to release neutrons that destroy the yields of ^{138}La and ^{180}Ta produced before. This is partly recovered by neutrino nucleosynthesis, where, however, only late neutrinos contribute. Similar to the production of ^{11}B in the lower He shell discussed above, here Approaches 1a and 1b are less effective in the production of ^{138}La than Approach 2, because the average neutrino energies at late times are below the time-averaged value. The maximum at the bottom of the O/Ne shell reflects yields which are predominantly produced by the γ process (Sieverding et al. 2018). Here, the contribution of the ν process is relatively small and arises from late time neutrinos, hence the local mass fractions in Approaches 1a and 1b are slightly smaller than in Approach 2. For both nuclides, ^{138}La and ^{180}Ta , the region in the outer O/Ne shell contributes most to the neutrino nucleosynthesis. Approaches 1a and 1b hence give larger total yields than Approach 2 (see Table 3). In Approach 3 as well as in Sieverding et al. (2018) the production is also noticeably smaller because the ν_e -induced nucleosynthesis is strongly reduced, if the electron neutrinos emitted during the burst and accretion phases are not considered. As discussed in Sieverding et al. (2018), the $27 M_\odot$ progenitor model is special with respect to the ^{180}Ta production, because the yield predominantly results from a pre-supernova γ process.

4. EFFECTS OF PINCHED NEUTRINO SPECTRA

In the previous section we have already seen that including pinched neutrino spectra in terms of the pinching factor $\alpha(t)$ in Equation (4) in our Approach 1a slightly reduces the production of the ν -process nuclei compared to Approach 1b, which uses a constant value of $\alpha = 2.3$. To illustrate the effect of the spectral pinching on the nucleosynthesis yields more clearly, we have performed a set of calculations which use the time-dependent neutrino luminosities and average energies from the simulation but keep the α parameter of the neutrino spectra defined in Equation (4) constant at a range of values. Figure 5 shows the yields that we obtain in the respective nucleosynthesis studies. We recall that the neutrino-nucleus cross section is reduced for larger values of α , i.e., high energy neutrinos are more suppressed, and that the reduction is more effective for larger reaction thresholds. These two ob-

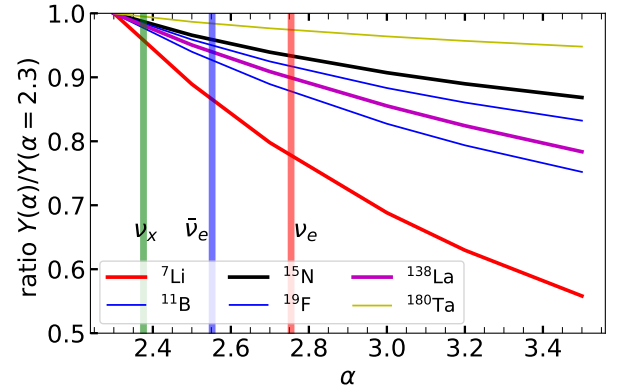


Figure 5. Dependence of production yields on the α parameter of the neutrino spectra. For each calculation, the same constant value of α was assumed for all neutrino species. The vertical lines indicate the averaged values from the simulations used in the previous section.

servations explain the results observed in Figure 5. The light nuclides are affected most as they involve reactions with Q -values of more than 10 MeV. The production of ^7Li , involving neutrino-induced reactions on ^4He and ^{12}C with their exceptionally large thresholds, is particularly sensitive. This can already be seen from the cross sections in Table 2. On the other hand, the $^{138}\text{Ba}(\nu_e, e^-)$ reaction needs to overcome only a Q -value of around 1 MeV and is therefore less dependent on the high-energy tail of the neutrino distribution than the neutral-current spallation reactions.

Whereas the general trend shows that the production of the light nuclides is most sensitive to the pinching of the neutrino spectra, the actual calculations using the spectral information from the supernova simulation give a different result. This can be seen from Table 3, comparing the yields obtained with the time-dependent, pinched spectra using $\alpha(t)$ from the supernova simulation (Approach 1a) to a calculation which assumes Fermi-Dirac-line spectra with $\alpha = 2.3$ for all neutrino species, as in previous studies, but also includes the time evolution of the average energies (Approach 1b). We find that the effect of taking into account $\alpha(t)$ is in general rather small and largest for the heavier isotope ^{138}La . The reason can be understood from the averaged α values, $\langle\alpha\rangle$, that are indicated as vertical lines in Figure 5 for the different neutrino species. Those values are obtained by taking the time average over $\alpha(t)$ from the supernova simulation as

$$\langle\alpha\rangle = \frac{1}{t_{\text{end}} - t_0} \int_{t_0}^{t_{\text{end}}} \alpha(t) dt, \quad (11)$$

where t_0 is the beginning of the neutrino emission around 50 ms before bounce and $t_{\text{end}} = 10$ s, at which time the neutrino luminosity has dropped below values relevant for nucleosynthesis. We find that the averaged α for ν_x ($\langle\alpha_{\nu_x}\rangle = 2.38$) and $\bar{\nu}_x$ ($\langle\alpha_{\bar{\nu}_x}\rangle = 2.26$) closely resembles Fermi-Dirac spectrum, whereas those for electron neutrinos ($\langle\alpha_{\nu_e}\rangle = 2.75$) and

electron antineutrinos ($\langle \alpha_{\bar{\nu}_e} \rangle = 2.55$) are slightly pinched. As a consequence of the spectral shape of ν_x and $\bar{\nu}_x$, the yields of those nuclides that are predominantly produced by neutral-current reactions change only little if neutrino spectra from the simulation are used rather than an FD-like spectrum ($\alpha = 2.3$).

Even though the relevant reaction cross section is not very sensitive to α , the synthesis of ^{138}La is affected the most by the pinching of the neutrino spectra, because it is produced by ν_e -induced charged-current reactions. Table 3 shows that a pinched neutrino spectra lead to a 7% reduction compared to the case of a FD-like spectra with $\alpha = 2.3$. This reduction agrees rather well with the results shown in Figure 5, where we find a 9% smaller value if we compare the yields calculated for the neutrino spectra with the averaged value for ν_e neutrinos to the ones for FD-like spectra². Since ^{180}Ta is made mainly in the pre-supernova stage, as discussed above, only the synthesis of ^{138}La is affected by the neutrino spectra for this progenitor model, because it is produced by ν_e -induced charged-current reactions. We stress, however, that this finding is specific to progenitor models like the one studied here. In less massive stars, ^{180}Ta is also produced via ν_e -induced neutrino reactions and should also be sensitive to the use of detailed neutrino spectra.

Neutrino oscillations, which we have neglected here, could lead to much more complicated spectral shapes (see e.g., Wu et al. 2015), and could also affect the nucleosynthesis yields.

5. SENSITIVITY TO THE BURST LUMINOSITY AND THE ACCRETION TIME

In this paper we have for the first time considered the electron neutrino burst and the standing accretion shock phase of a supernova explosion in a study of neutrino nucleosynthesis. Although both phases are firmly established in supernova simulations, some uncertainties about their properties still remain. In this section we will explore which impact these uncertainties have on the neutrino nucleosynthesis yields.

The existence of a ν_e burst is a well-established feature of supernova simulations which is not very sensitive to the progenitor model (Kachelrieß et al. 2005; Thompson et al. 2003). The maximum luminosity of the electron neutrino burst depends, however, on details of the nuclear equation of state and of the coupling of neutrinos to hot and dense nuclear matter. This introduces some uncertainties. For example, studies by Marek (2003) and Janka et al. (2004) have shown that the peak luminosity can vary by around 50 %, typically in the range $350\text{--}450 \times 10^{51} \text{ erg s}^{-1}$, when different nuclear equations of state are used.

² The small difference results from the fact that the results shown in Figure 5 assume constant $\alpha \geq 2.3$ for all neutrino species, whereas Approach 1a uses the values $\alpha(t)$ from the simulation.

We study the impact of this uncertainty by varying the neutrino burst peak luminosity. To this end, we fold the numerical electron neutrino luminosities $L_{\nu_e}^0(t)$ with a Lorentzian centered around the time of maximum luminosity, t_{burst} , i.e., we assume

$$L_{\nu_e}(t) = L_{\nu_e}^0(t) \left[1 + (A - 1) \frac{w^2}{(t - t_{\text{burst}})^2 + w^2} \right], \quad (12)$$

with a half-width, w , of 12.5 ms and a variable enhancement factor, A . Using this ansatz, the enhancement factor directly translates into an increase of the peak luminosity by a factor, $A > 1$. The width of the enhancement is chosen such that the effect is limited to the duration of the neutrino burst. The modification is illustrated by the red dashed line in Figure 6. In our calculation, we assume that neither the luminosities of the other neutrino species nor the neutrino spectra are modified by the variation of the burst luminosity. Figure 7 shows the relative yields of the ν -process nuclides as a function of the enhancement factor, A . Even though we do not expect to find variations of the peak luminosities in supernova simulations by more than 50%, we vary A by up to a factor 4 for illustrative purposes. The yields increase by enhancing the burst luminosity and in the regime we study, this is a linear effect, which overall, however, is small. The neutrino burst has an impact on the yields of nuclides which are produced by ν_e -induced charged-current reactions. Thus, we observe the largest changes due to variations of the burst luminosity for ^{138}La . For progenitors with different masses we expect the ^{180}Ta yield to show a similar dependence. We note again, that the current 27 M_\odot progenitor model represents an exception for the ^{180}Ta production, as it is synthesized by a pre-explosive γ process (e.g., Rauscher et al. 2002) and not by ν_e -induced charged-current reactions, as for other progenitor stars (Sieverding et al. 2018). Consequently, the ^{180}Ta yield in Figure 7 shows very little variation when the burst luminosity is increased. Effects of the variation of the burst luminosity on the yields of ^7Li , ^{15}N and ^{19}F are negligible, because these isotopes are mainly produced by neutral-current reactions. Half of the ^{11}B production in the C/O shell, which constitutes a major part of the total yield, results from charged-current reactions and hence ^{11}B shows some sensitivity to the variation of the burst luminosity. The electron neutrino spectra are strongly pinched during the neutrino burst (see Figure 1), i.e., the high energy tail is significantly reduced compared to an FD-like spectrum with $\alpha = 2.3$. As a consequence the impact of the neutrino burst on the neutrino nucleosynthesis yields is noticeably reduced, if—like in the present work—pinched neutrino spectra are considered rather than Fermi-Dirac spectra. This can be seen by comparing the left panel of Figure 7, which is calculated with the time-dependent $\alpha(t)$, to the right panel, where FD-like spectra have been assumed.

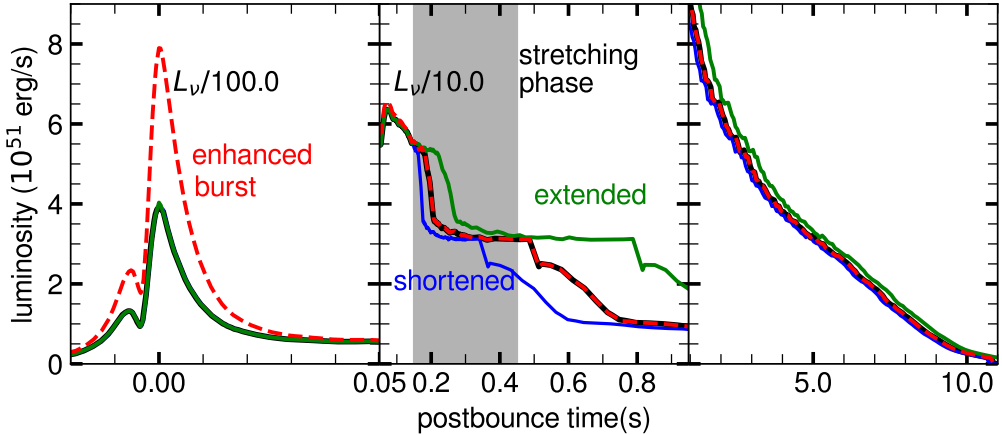


Figure 6. Neutrino luminosities that illustrate the modifications applied to the neutrino signal. The shaded region indicates the time interval in which the data were stretched in order to achieve the modification of the accretion period.

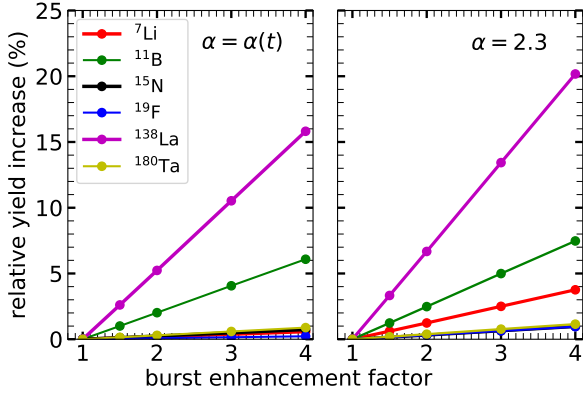


Figure 7. Effect of the variation of the peak luminosity of the electron neutrino burst at shock breakout by Equation (12) for the $27 M_{\odot}$ model. The left panel shows the results including the effects of pinched neutrino spectra and for the results shown in the right panel a constant value of $\alpha = 2.3$ has been assumed, approximating pure FD spectra. The pinching reduces the effect of the ν_e burst enhancement.

Another qualitatively well-established, but quantitatively uncertain feature of the supernova neutrino emission is the accretion phase. Müller (2015) and Bruenn et al. (2016) have reported simulations in which accretion-driven neutrino emission can persist for up to ~ 1 s after core bounce. After a successful shock revival, the mass accretion rate drops substantially also in multi-D simulations and the neutrino emission is reduced. Most modern simulations predict a delay time until shock revival of a few hundred milliseconds after core bounce. The duration of this phase of accretion until the onset of the explosion is subject to the treatment of multi-dimensional turbulence that might not be fully numerically resolved yet (Radice et al. 2016), even in state-of-the-art three-dimensional simulations. The duration is also sensitive to the neutrino interactions in nuclear matter (O'Connor & Couch 2018; Burrows et al. 2018).

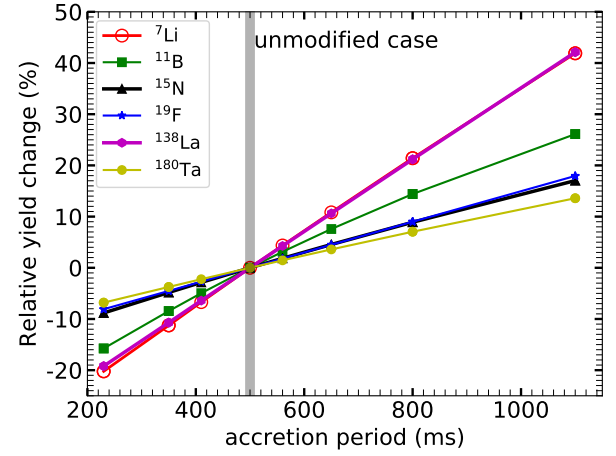


Figure 8. Relative change of the production of ν -process nuclei due to the variation of the duration of the accretion phase as illustrated in Figure 6. The grey vertical bar indicates the result for the original, unmodified neutrino data. The production factor of ^{138}La exceeds a production factor of unity for an accretion period of 1100 ms.

Here we explore the sensitivity of the ν -process nucleosynthesis to the delay time until shock revival and thus the duration of the phase of most vigorous accretion. In order to do so, we have modified the neutrino signal shown in Figure 1, which has been the default of our calculations so far (Approach 1a), by stretching the time steps in the interval between 0.15 s and 0.45 s to vary the length of the accretion phase. The same time stretching has been applied to the neutrino energies and $\alpha(t)$. In practice, we have replaced each value t_i of the temporal grid of the simulation dumps by $t'_i = t'_{i-1} + f_s (t_i - t_{i-1})$, where i runs over the simulation dumps with $0.15 \text{ s} < t_i < 0.45 \text{ s}$ and f_s is a stretching factor. Outside the stretching interval the timesteps are left unchanged with an offset to compensate the modifications. This is also illustrated in Figure 6 by the blue and green lines. In

this way, we can mimic a variation of the delay time without making any further assumptions about the structure of the signal. Physically, this variation can be associated with a modification of the mass accretion rate, that is sensitive to the complex dynamics of multi-dimensional fluid flows. Figure 8 shows the enhancement of the yields of the ν -process nuclides as function of the modified duration of the accretion phase. The results obtained for an accretion period of 500 ms as adopted throughout this paper so far, is indicated by the gray vertical bar. The yields grow with increasing length of the accretion phase. During the accretion phase the ν_e luminosity is noticeably larger than the ν_x luminosity and, on average, the ν_e spectra are shifted to higher energies compared to the later phases. This shift is larger for ν_e than for the other neutrino species. Both effects favor charged-current over neutral-current reactions. As a consequence, the production of ^{138}La can be noticeably enhanced if the accretion phase lasts longer. (For the reasons discussed above, we expect a similar effect for ^{180}Ta in other progenitor stars.) This effect is even underestimated in the current treatment, because $\langle E_{\nu_e} \rangle$ and $\langle E_{\bar{\nu}_e} \rangle$ are expected to continue to rise during a longer accretion period in self-consistent models. The yield of ^7Li also grows noticeably in relative terms with the length of the accretion phase. This is related to the fact that ^7Li is mostly produced at large radii in the He shell, where the shock heating is not significant and the whole neutrino signal can come to bear. For both, ^7Li and ^{11}B charge-current reactions, which are the most enhanced by an extended accretion period, contribute about 50 % of the total production. The production ^{11}B in the O/C shell, however, is less sensitive to the early neutrino emission, because of the stronger shock heating (see Figure 3). In general, the yields for nuclides which are mainly produced by neutral-current reactions, are less sensitive to the duration of the accretion phase. The electron flavor neutrinos also induce particle emission by neutral-current scattering. However, due to their lower energies their contribution is typically small compared to the heavy flavor neutrinos. For example, the charged-current reactions $(\nu_e, e^- p)$ and $(\bar{\nu}_e, e^+ n)$ on ^{20}Ne and ^{16}O also contribute to the yields of ^{19}F and ^{15}N , respectively, but their production is increased by less than 10% even if the accretion period lasts for more than 1 s. A shortened accretion phase reduces the yields of ^7Li and ^{138}La substantially. A reduction of the delay time of the explosion to around 200 ms would reduce the production factor of ^{138}La normalized to ^{16}O down to 0.5. Assuming that supernovae are the main production site of ^{138}La , very fast or even prompt supernova explosions would make it more difficult to explain the solar abundance of ^{138}La . A prolonged accretion phase, on the other hand, selectively increases the production of the heavier elements without risking an overproduction of the light elements ^7Li , ^{11}B , ^{15}N , and ^{19}F . Recent studies by [Travaglio et al. \(2011\)](#)

and [Travaglio et al. \(2018\)](#) suggest that a substantial fraction of ^{180}Ta could also come from the γ process in Type Ia supernovae with strong, accretion-induced *s*-process enrichment, but they do not find a significant contribution to ^{138}La . This leaves ^{138}La as a good candidate that could be a clear indicator of the ν process in core-collapse supernovae. We note that the duration of the accretion phase can noticeably enhance the production factor of ^{138}La (and, as we expect, for ^{180}Ta for other progenitor stars). As both yields are close to the solar production factors, an additional production due to an extended accretion phase might generate some tension due to overproduction. For the $27 M_\odot$ model studied here, the production factor of ^{138}La exceeds unity only for an extremely long accretion period of 1100 ms. Such a long delay time is currently not predicted by simulations making them consistent with the solar ^{138}La abundance.

More quantitative statements, however, require to extend our study to the full range of supernova progenitor models with a consistent treatment of the neutrino emission.

6. CONCLUSIONS

We have performed neutrino nucleosynthesis calculations for a $27 M_\odot$ stellar progenitor model that, for the first time, use time-dependent neutrino emission spectra as obtained from modern (one-dimensional) supernova simulations. In particular, our approach includes the neutrino emission during the early electron neutrino burst and accretion phases of the explosion. Furthermore, we use the spectral form of emitted neutrinos as predicted by the simulations, and hence account for their deviations from a zero degeneracy Fermi-Dirac spectrum, which has been the default assumption in previous studies of ν -process nucleosynthesis.

Our calculations confirm that selected nuclides (^7Li , ^{11}B , ^{15}N , ^{19}F , ^{138}La , and ^{180}Ta) are partly or predominantly produced by the ν process. The production of the nuclei ^{138}La and ^{180}Ta is mainly due to ν_e -induced charged-current reactions, whereas neutral-current reactions, induced mainly by the neutrino species other than electron neutrinos due to their higher average energies, contribute to the ν -process yields of the other four nuclides. We find that our calculation with time-dependent neutrino emission spectra results in noticeably higher yields than obtained in the spirit of previous approaches, i.e., assuming constant neutrino average energies appropriate for the neutrino emission from the proto-neutron star cooling phase. In an additional approach, we have shown that the yields obtained with the fully time-dependent neutrino emission can be reproduced within a few percent if the constant average energy takes into account the full neutrino emission including the neutrino burst and accretion phases.

We have found that the electron neutrino burst gives a rather small contribution to the total ν -process yields, even for those nuclides produced by ν_e charged-current reactions.

Neutrino emission during the accretion phase has a larger impact on the total yields, enhancing the production between about 5 % for nuclides made by neutral-current reactions and nearly 20 % for those with strong charged-current contributions, caused by the relatively high luminosities and average energies of electron neutrinos during the accretion phase. In this paper we used the neutrino emission spectra from the supernova simulation of Mirizzi et al. (2016), in which the accretion phase lasts for around 500 ms. There is, however, some uncertainty about the duration of the accretion period. We have shown that the production of ^{138}La increases by more than 40 % if vigorous accretion-induced neutrino emission lasts for one second.

The calculated neutrino spectra deviate from a Fermi-Dirac distribution. This deviation is quite strong during the burst phase where the electron neutrino spectra are strongly pinched, i.e., shifted to smaller energies. This is one reason why the electron neutrinos emitted during the burst have a small impact on the ν -process yields. Overall, the consideration of pinched spectra has a negligible effect on the neutrino nucleosynthesis results. The main reason is that the spectra during the cooling phase are well approximated by a Fermi-Dirac distribution.

We have shown that the outcome of neutrino nucleosynthesis in general, and of our improved time-dependent treatment of neutrino emission in particular, is a subtle competition of neutrino-induced reactions and the effect of the shock wave. The competition depends sensitively on the radial position in the star at which the nucleosynthesis occurs. As the neutrinos travel faster than the shock, parts of the neutrino nucleosynthesis has already happened when the shock arrives. The shock can destroy this abundance if the associated temperatures are high enough. Importantly, the radial position in the star, i.e., the time at which the shock operates, also decides which temporal portion of the neutrino emission can induce nucleosynthesis reactions after the passage of the shock. As later emitted neutrinos have smaller average energies, their contributions to the ν -process yields is reduced, in particular compared to studies which assume constant neutrino average energies.

In general, we have demonstrated that a proper treatment of the time-dependent neutrino emission has a significant impact on the neutrino nucleosynthesis yields. Such a treatment

is hence indispensable if one wants to use neutrino nucleosynthesis as a thermometer for supernova neutrino emission (e.g., Heger et al. 2005), or even, to constrain neutrino properties like mass hierarchy of mixing angles (see Yoshida et al. 2005, 2006; Kajino et al. 2014). Yet, we also see some necessary next steps. Our calculation has been restricted to a $27 M_{\odot}$ progenitor star, consistent with the supernova simulation (which, however, has quite exceptional features for the ν -process production of ^{180}Ta). Additional calculations for the broad range of progenitors which contribute to the galactic chemical evolution are desirable. At this point we have also neglected neutrino flavor conversion effects on the ν process. Finally, our study is based on the neutrino emission data obtained from a one-dimensional supernova simulation. Thus, it does not properly describe effects on the neutrino emission which are caused or influenced by multi-dimensional phenomena. Such improvements, which are particularly relevant for the accretion phase, will be the subject of future studies.

This work was supported in part by the US Department of Energy [DE-FG02-87ER40328 (UM)]. GMP is partly supported by the Deutsche Forschungsgemeinschaft (DFG, German Research Foundation) - Projektnummer 279384907 - SFB 1245 “Nuclei: From Fundamental Interactions to Structure and Stars” and the “ChETEC” COST Action (CA16117), funded by COST (European Cooperation in Science and Technology). At Garching, this project was supported by the European Research Council through grant ERC-AdG No. 341157-COCO2CASA, and by the Deutsche Forschungsgemeinschaft through Sonderforschungsbereich SFB 1258 “Neutrinos and Dark Matter in Astro- and Particle Physics” (NDM) and the Excellence Cluster Universe (EXC 153; <http://www.universe-cluster.de/>). The neutrino data of RB’s simulation is available through the core-collapse supernova archive <https://wwwmpa.mpa-garching.mpg.de/ccsnarchive/archive.html>. AH was supported by an Australian Research Council (ARC) Future Fellowship (FT120100363), by the US National Science Foundation under Grant No. PHY-1430152 (JINA Center for the Evolution of the Elements and by TDLI/SJTU though a grant from Science and Technology Commission of Shanghai Municipality (grant No. 16DZ2260200) and National Natural Science Foundation of China (grant No.11655002).

REFERENCES

Arnould, M., & Goriely, S. 2003, PhR, 384, 1
 Asplund, M., Grevesse, N., Sauval, A. J., & Scott, P. 2009,
 ARA&A, 47, 481
 Audi, G., Kondev, F. G., Wang, M., Huang, W. J., & Naimi, S.
 2017, ChPhC, 41, 030001
 Austin, S. M., Heger, A., & Tur, C. 2011, PhRvL, 106, 152501
 Balasi, K., Langanke, K., & Martínez-Pinedo, G. 2015, PrPNP, 85,
 33
 Banerjee, P., Qian, Y.-Z., Heger, A., & Haxton, W. C. 2016, Nature
 Communications, 7, 13639
 Bartl, A., Bollig, R., Janka, H.-T., & Schwenk, A. 2016, PhRvC,
 94, 083009

Bruenn, S. W., Lentz, E. J., Hix, W. R., et al. 2016, *ApJ*, 818, 123

Burrows, A., Vartanyan, D., Dolence, J. C., Skinner, M. A., & Radice, D. 2018, *SSRv*, 214, 33

Cheoun, M.-K., Ha, E., Hayakawa, T., et al. 2012, *PhRvC*, 85, 065807

Cooperstein, J. 1988, *PhR*, 163, 95

Curtis, S., Ebinger, K., Fröhlich, C., et al. 2019, *ApJ*, 870, 2

Cyburt, R. H., Amthor, A. M., Ferguson, R., et al. 2010, *ApJS*, 189, 240

Fröhlich, C., Martínez-Pinedo, G., Liebendörfer, M., et al. 2006, *PhRvL*, 96, 142502

Giovanoni, P. M., Ellison, D. C., & Bruenn, S. W. 1989, *ApJ*, 342, 416

Hayakawa, T., Mohr, P., Kajino, T., Chiba, S., & Mathews, G. J. 2010, *PhRvC*, 82, 058801

Heger, A., Kolbe, E., Haxton, W., et al. 2005, *Phys. Lett. B*, 606, 258

Huther, L. 2014, PhD thesis, TU Darmstadt

Janka, H.-T. 2001, *A&A*, 368, 527

Janka, H.-T., Buras, R., Kitaura, F. S., et al. 2004, in Proceedings of 12th Workshop on Nuclear Astrophysics, Ringberg Castle, Tegernsee, ed. E. Müller & H.-T. Janka, 150

Janka, H.-T., & Hillebrandt, W. 1989, *A&A*, 224, 49

Janka, H.-T., Langanke, K., Marek, A., Martínez-Pinedo, G., & Müller, B. 2007, *PhR*, 442, 38

Janka, H.-T., Melson, T., & Summa, A. 2016, *ARNPS*, 66, 341

Kachelrieß, M., Tomàs, R., Buras, R., et al. 2005, *PhRvC*, 71, 063003

Kajino, T., Mathews, G. J., & Hayakawa, T. 2014, *JPhG*, 41, 044007

Keil, M. T., Raffelt, G. G., & Janka, H.-T. 2003, *ApJ*, 590, 971

Kolbe, E., Langanke, K., Krewald, S., & Thielemann, F.-K. 1992, *NuPhA*, 540, 599

Kolbe, E., Langanke, K., Martínez-Pinedo, G., & Vogel, P. 2003, *JPhG*, 29, 2569

Langanke, K., & Kolbe, E. 2001, *ADNDT*, 79, 293

Langanke, K., Vogel, P., & Kolbe, E. 1996, *PhRvL*, 76, 2629

Liebendörfer, M., Rampp, M., Janka, H.-T., & Mezzacappa, A. 2005, *ApJ*, 620, 840

Lodders, K. 2003, *ApJ*, 591, 1220

Lodders, K., Palme, H., & Gail, H.-P. 2009, *Landolt Börnstein*, 712

Marek, A. 2003, PhD thesis, Diploma thesis, Technische Universität München (TUM)

Mirizzi, A., Tamborra, I., Janka, H.-T., et al. 2016, *Riv. del Nuovo Cim.*, 39, 1

Mohr, P., Käppeler, F., & Gallino, R. 2007, *PhRvC*, 75, 012802

Möller, P., Pfeiffer, B., & Kratz, K.-L. 2003, *PhRvC*, 67, 055802

Müller, B. 2015, *MNRAS*, 453, 287

Müller, B., Heger, A., Liptai, D., & Cameron, J. B. 2016, *MNRAS*, 460, 742

Myra, E. S., & Burrows, A. 1990, *ApJ*, 364, 222

O'Connor, E., Bollig, R., Burrows, A., et al. 2018, *JPhG*, 45, 104001

O'Connor, E. P., & Couch, S. M. 2018, *ApJ*, 854, 63

Pignatari, M., Herwig, F., Hirschi, R., et al. 2016, *ApJS*, 225, 24

Prantzos, N., Abia, C., Limongi, M., Chieffi, A., & Cristallo, S. 2018, *MNRAS*, 476, 3432

Radice, D., Abdikamalov, E., Ott, C. D., et al. 2018, *JPhG*, 45, 053003

Radice, D., Ott, C. D., Abdikamalov, E., et al. 2016, *ApJ*, 820, 76

Rampp, M., & Janka, H.-T. 2002, *A&A*, 396, 361

Rauscher, T., Heger, A., Hoffman, R. D., & Woosley, S. E. 2002, *ApJ*, 576, 323

Scholberg, K. 2012, *ARNPS*, 62, 81

Sieverding, A., Martínez-Pinedo, G., Huther, L., Langanke, K., & Heger, A. 2018, *ApJ*, 865, 143

Steiner, A. W., Hempel, M., & Fischer, T. 2013, *ApJ*, 774, 17

Sukhbold, T., Ertl, T., Woosley, S. E., Brown, J. M., & Janka, H.-T. 2016, *ApJ*, 821, 38

Tamborra, I., Müller, B., Hüdepohl, L., Janka, H.-T., & Raffelt, G. 2012, *PhRvC*, 86, 125031

Thompson, T. A., Burrows, A., & Pinto, P. A. 2003, *ApJ*, 592, 434

Travaglio, C., Rauscher, T., Heger, A., Pignatari, M., & West, C. 2018, *ApJ*, 854, 18

Travaglio, C., Röpke, F. K., Gallino, R., & Hillebrandt, W. 2011, *ApJ*, 739, 93

Wanajo, S., Müller, B., Janka, H.-T., & Heger, A. 2018, *ApJ*, 852, 40

Woosley, S. E., Hartmann, D. H., Hoffman, R. D., & Haxton, W. C. 1990, *ApJ*, 356, 272

Woosley, S. E., & Heger, A. 2007, *PhR*, 442, 269

Woosley, S. E., Heger, A., & Weaver, T. A. 2002, *RMP*, 74, 1015

Woosley, S. E., & Weaver, T. A. 1995, *ApJS*, 101, 181

Wu, M.-R., Qian, Y.-Z., Martínez-Pinedo, G., Fischer, T., & Huther, L. 2015, *PhRvC*, 91, 065016

Yoshida, T., Kajino, T., & Hartmann, D. H. 2005, *PhRvL*, 94, 231101

Yoshida, T., Kajino, T., Yokomakura, H., et al. 2006, *ApJ*, 649, 319

Yoshida, T., Suzuki, T., Chiba, S., et al. 2008, *ApJ*, 686, 448